

Time-optimal synchronisation to self-sustained oscillations under bounded control

C. Ríos-Monje,¹ C. A. Plata,¹ D. Guéry-Odelin,² and A. Prados¹

¹*Física Teórica, Multidisciplinary Unit for Energy Science, Universidad de Sevilla, Apartado de Correos 1065, E-41080 Sevilla, Spain*

²*Laboratoire de Collisions Agrégats Réactivité, Université de Toulouse, CNRS, 118 Route de Narbonne, 31062 Toulouse CEDEX 4, France*

(Dated: July 29, 2025)

Incorporating force bounds is crucial for realistic control implementations in physical systems. In this Letter, we investigate the fastest possible synchronisation of a Liénard system to its limit cycle using a bounded external force. To tackle this challenging non-linear optimal control problem, our approach involves applying Pontryagin’s Maximum Principle with a combination of analytical and numerical tools. We show that the optimal control develops a remarkably complex structure in phase space as the force bound is lowered. Trajectories rewound from the limit cycle’s extreme points turn out to play a key role in determining the maximum number of control bangs for optimal connection. We illustrate these intricate features using the paradigmatic van der Pol oscillator model.

Self-sustained oscillations are a type of oscillatory behaviour that persists over time without any external driving [1, 2]. This phenomenon is ubiquitous in nature, playing a fundamental role in many fields: active membranes [3], climate change [4], cancer cell dynamics [5], circadian rhythms [6–8], electronic resonators [9–11], network dynamics [12, 13], or quantum devices [14]. Within this context, the Liénard equation describes a broad family of non-linear oscillators [15], including van der Pol’s [16], that exhibit such self-sustained oscillations.

Generally, self-sustained oscillations are only achieved in the infinite time limit, appearing as stable limit cycles in the phase space of the system [17]. Both from a theoretical and a practical point of view, it is relevant to look into the synchronisation of the system to its limit cycle in a finite time, by applying an external force. This is a problem that has only very recently been addressed, specifically for the van der Pol oscillator when arbitrarily large values of the force are possible. Using ideas imported from the field of shortcuts, first developed for quantum systems [18] and later transposed to classical systems, both with deterministic and stochastic dynamics [19], non-optimal connections [20] and protocols minimising the energetic cost [21] have been analysed. Interestingly, the latter protocol involves Dirac-delta peaks of the force at the initial and final times [21], similarly to the situation found in stochastic thermodynamics for underdamped systems [22, 23].

In any actual physical system, the applied driving $F(t)$ force is bounded—in the simplest scenario, by the non-holonomic constraint $|F(t)| < K$. Aside from limiting the practical applicability of protocols with impulsive forces, like those in Refs. [21, 22], the force bounds entail a minimum time is expected to emerge for the protocol. Driving the system as fast as possible to its long-time state is especially relevant in the limit of small dissipation, in which the natural relaxation time becomes very long.

In the quantum context, minimum time connections are related to the quantum speed limit and the quan-

tum brachistochrone problem, i.e. finding the protocol that connects given initial and final states in the shortest time [24–28]. Similar minimum time problems have been recently explored in many fields, e.g. [29, 30]; in the specific context of non-equilibrium statistical mechanics, minimum time protocols have been analysed for connecting equilibrium states and also non-equilibrium steady states [23, 31, 32]. Yet, optimising the connection towards a time-dependent state in the presence of a non-holonomic constraint remains a challenge.

In this work, we address the above challenge by optimising, in terms of connection time, the synchronisation of the general class of non-linear oscillators described by the Liénard equation to its limit cycle, by applying a bounded external force. Optimal control theory is the mathematical framework to address this problem. Specifically, we are dealing with a minimum time problem, which can be solved using Pontryagin’s Maximum Principle (PMP) [25, 33, 34]. PMP provides necessary conditions for the optimal control, i.e. the optimal driving force that minimises the connection time to the limit cycle and the corresponding optimal trajectory of the system in phase space.

After presenting the Liénard equation, we seek the fastest synchronisation to its limit cycle. PMP allows us to derive key analytical results and find the general structure of the optimal driving: the optimal protocol is always bang-bang, alternating time windows with $F(t) = \pm K$. Notably, a very complex optimal control structure emerges as the bound decreases, with an increasing number of bangs. Though the analytical results are derived for the general Liénard equation, we always illustrate numerical results using the paradigmatic van der Pol oscillator.

Model– The Liénard equation [15, 35–44] describes a wide family of non-linear oscillators with potential $V(x)$ and non-linear damping force $-\mu h(x)\dot{x}$:

$$\ddot{x} + \mu h(x)\dot{x} + V'(x) = 0, \quad (1)$$

where μ is a constant called damping coefficient, and $h(x) \in \mathcal{C}^1$ and $V(x) \in \mathcal{C}^2$ are even functions. Equation (1) is written in dimensionless variables. It has a unique and stable limit cycle, denoted by $\chi_{\ell c}(x, \dot{x}; \mu) = 0$, under quite general conditions [45].

Our goal is to synchronise this system, i.e. to drive it from an arbitrary initial condition to its self sustained oscillations in a finite time by applying an external driving force $F(t)$. Thus, we add $F(t)$ to the right-hand-side (rhs) of Eq. (1). The resulting driven Liénard equation is conveniently rewritten in phase space, introducing $\mathbf{x}^T(t) \equiv (x_1(t), x_2(t))$, $x_1 = x$, $x_2 = \dot{x}$, as

$$\dot{\mathbf{x}} \equiv \begin{pmatrix} \dot{x}_1 \\ \dot{x}_2 \end{pmatrix} = \mathbf{f}(\mathbf{x}, F) \equiv \begin{pmatrix} x_2 \\ -\mu h(x_1)x_2 - V'(x_1) + F \end{pmatrix}. \quad (2)$$

Among all possible solutions of the synchronisation problem, we are interested in that minimising the time taken to reach the limit cycle when the force is bounded,

$$|F(t)| \leq K, \quad \forall t > 0. \quad (3)$$

Therefore, the optimisation problem to be solved is

$$\min_{\mathbf{x} \in \mathcal{C}^1, |F(t)| \leq K} t_f = \int_0^{t_f} dt, \quad (4)$$

where the system dynamics verifies Eq. (2), the initial phase-space point is fixed, and the final phase-space point $\mathbf{x}_f \equiv \mathbf{x}(t_f)$ belongs to the limit cycle,

$$\mathbf{x}^T(0) = (x_{10}, x_{20}), \quad \chi_{\ell c}(\mathbf{x}_f; \mu) = 0. \quad (5)$$

Since the limit cycle is a closed curve in phase space, the latter is split into two regions: (i) interior points, chosen to be defined by $\chi_{\ell c}(\mathbf{x}; \mu) < 0$ and (ii) exterior points, where $\chi_{\ell c}(\mathbf{x}; \mu) > 0$.

PMP provides the necessary conditions for determining the optimal control $F^*(t)$ (here, the driving force) that minimises the connection time, along with the corresponding optimal trajectory $\mathbf{x}^*(t)$ over the time interval $t \in [0, t_f]$. At its core, PMP relies on the definition of the Pontryagin Hamiltonian \mathcal{H} , given by:

$$\begin{aligned} \mathcal{H}(\mathbf{x}, \mathbf{p}, p_0; F) &= \mathbf{p} \cdot \mathbf{f}(\mathbf{x}, F) + p_0 \\ &= p_1 f_1(\mathbf{x}, F) + p_2 f_2(\mathbf{x}, F) + p_0. \end{aligned} \quad (6)$$

According to PMP, there exists a costate vector $\mathbf{p}^*(t)$, also defined in the time interval $t \in [0, t_f]$, and a constant $p_0^* \leq 0$, with $\{\mathbf{p}^*, p_0^*\} \neq \{\mathbf{0}, 0\}$ for all $t \in [0, t_f]$. These satisfy the following three conditions, (i) canonical system equations: the time evolution of $\{\mathbf{x}(t), \mathbf{p}(t)\}$ is governed by

$$\dot{\mathbf{x}}^* = \nabla_{\mathbf{p}^*} \mathcal{H}^*, \quad \dot{\mathbf{p}}^* = -\nabla_{\mathbf{x}^*} \mathcal{H}^*, \quad (7)$$

together with the boundary conditions given in Eq. (5); (ii) Hamiltonian maximisation condition: $\forall t \in [0, t_f]$ and

$\forall F \in [-K, +K]$, \mathcal{H} attains its maximum value, which is zero, as a function of the driving force at F^* ,

$$\mathcal{H}(\mathbf{x}^*, \mathbf{p}^*, p_0^*; F) \leq 0 = \mathcal{H}^* \equiv \mathcal{H}(\mathbf{x}^*, \mathbf{p}^*, p_0^*; F^*), \quad (8)$$

and (iii) transversality condition at the final time t_f : the costate vector is orthogonal to the tangent space of the limit cycle,

$$\mathbf{p}_f^* \cdot \mathbf{d} = 0, \quad \forall \mathbf{d} \in T_{\mathbf{x}_f^*} \{\chi_{\ell c} = 0\}. \quad (9)$$

Asterisks are dropped hereafter, as all variables refer to the optimal solution.

PMP provides a framework for determining the optimal driving force and solving the minimum time synchronisation problem. However, the non-linearity of the involved equations prevent us from obtaining a full analytical solution for the optimal protocol. Yet, our analysis of PMP makes it possible to discern the structure of the optimal driving force, also enabling us to obtain a complete solution of the optimisation problem numerically.

Main results—We now present the main results for the minimum time problem stemming from PMP; detailed derivations are in the Appendix. Remarkably, all results apply for the wide class of non-linear oscillators described by the Liénard equation.

1. A key PMP result is the bang-bang nature of the optimal driving force: it only takes extreme values, either $F(t) = -K$ or $F(t) = +K$. In particular, we have

$$F(t) = \text{sgn}(p_2(t))K, \quad (10)$$

where p_2 is the second component of the costate \mathbf{p} . The force changes discontinuously from $F(t) = \pm K$ to $\mp K$ at the times t_s such that $p_2(t_s) = 0$, which determine these switching points. Our numerical analysis, detailed below, demonstrates that decreasing the bound K increases the number of bangs, leading to a very complex optimal control structure.

2. The final costate \mathbf{p}_f is obtained by combining Eqs. (8) and (9) at $t = t_f$. Two cases can be distinguished:

- (i) $(x_{1f}, x_{2f}) \neq (\pm x_{\ell c}^{\max}, 0)$:
$$p_{1f} = \frac{\mu h(x_{1f})x_{2f} + V'(x_{1f})}{F_f x_{2f}}, \quad p_{2f} = \frac{1}{F_f}, \quad p_0 = -1, \quad (11a)$$

- (ii) $(x_{1f}, x_{2f}) = (\pm x_{\ell c}^{\max}, 0)$:
$$p_{1f} = \text{sgn}(F_f), \quad p_{2f} = 0, \quad p_0 = 0, \quad (11b)$$

where $(\pm x_{\ell c}^{\max}, 0)$ are the extreme points of the limit cycle over the x_1 -axis.

3. Let us examine optimal trajectories that end at the limit cycle's extreme points—i.e. case (ii) of result 2, Eq. (11b), which we call critical trajectories. Over the

critical trajectories, all switching points lie on the x_1 -axis: since $p_0 = 0, \forall t$, and at the switching points $p_2(t_s) = 0$, Eqs. (6) and (8) entail $x_2(t_s) = 0$ —PMP excludes the possibility $p_1(t_s) \neq 0$. Note that the reverse statement is also true: over the critical trajectories, points lying on the x_1 -axis are switching points.

4. The sign of the force in the final bang can be inferred by analysing the behaviour of $\chi_{\ell c}$ around the final time, as a function of $\text{sgn}(x_{2f})$ and the position of the initial point with respect to the limit cycle. Let us define $x_{2f}^- \equiv x_2(t_f^-)$. For initial points outside the limit cycle, we have: (a) for $x_{2f}^- < 0$, the final value of the force is $F_f > 0$ and thus the last bang corresponds to $F(t) = +K$, (b) for $x_{2f}^- > 0$, $F_f < 0$ and the last bang corresponds to $F(t) = -K$. For points inside the limit cycle, the above cases are reversed.

The analytical results 1–4 above allow us to determine the final conditions of any possible optimal trajectory. These are crucial to obtain a complete numerical solution for the optimisation problem, which we describe below.

Numerical analysis—Building on the just presented analytical results, we carry out a complete numerical solution of the optimisation problem. Specifically, we present results for the van der Pol oscillator, a paradigmatic case of the Liénard equation with the choice $h(x) = x^2 - 1$, $V(x) = x^2/2$. The van der Pol equation and some variants have been employed in many different contexts, such as electronic simulation of nervous impulses [46, 47], elastic excitable media [48], solar cycle [49], active matter [50], light-matter interaction [51], or synchronisation of quantum systems [20, 52–55].

Our numerical approach consists in a backward integration from any final point $\mathbf{x}_f^T = (x_{1f}, x_{2f})$ over the limit cycle. Equation (11) determines the final value of the momenta and result 4 above determines the final bang, which allows us to numerically solve Eq. (7) backward in time from $t = t_f$. Following Eq. (10), every time p_2 changes its sign, F also changes. Starting from all points over the limit cycle, we obtain all the possible trajectories fulfilling PMP. Finally, to determine the optimal solution for any initial phase space point $\mathbf{x}_0^T = (x_{10}, x_{20})$, we have two cases: (i) if there is only one trajectory containing \mathbf{x}_0 , then it is the optimal solution; or (ii) if there are multiple trajectories containing \mathbf{x}_0 , we choose that reaching the limit cycle the fastest.

To carry out a systematic thorough analysis of the candidates to optimal protocols, we divide the phase plane in two regions: outside the limit cycle, $\chi_{\ell c} > 0$, and inside the limit cycle, $\chi_{\ell c} < 0$. All numerical results correspond to a damping coefficient $\mu = 0.1$, for which the dimensionless relaxation time to the limit cycle is $t_R \simeq 40$ [21].

Exterior points—First, we focus on the region outside the limit cycle. Result 4 for the final bang, particularised to the van der Pol equation, tells us $\text{sgn}(F_f) = -\text{sgn}(x_{2f})$ if $x_{2f} \neq 0$, whereas $\text{sgn}(F_f) = -\text{sgn}(x_{1f})$ if $x_{2f} = 0$.

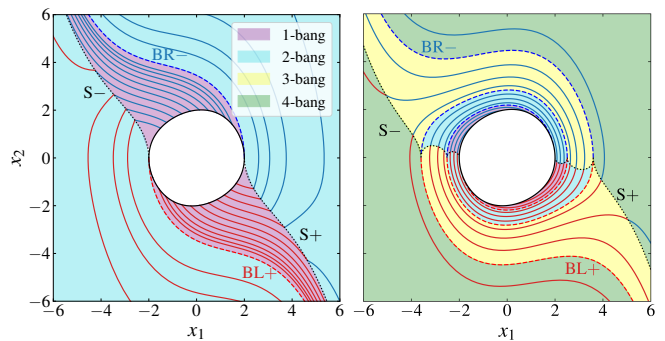


FIG. 1. Optimal trajectories for initial phase space points outside the limit cycle. Force bounds are: $K = 2$ (left) and $K = 0.2$ (right), for which the maximum number of bangs is two and four, respectively. The curves delimiting the different regions in phase space are plotted: the switching curves $S+$ and $S-$, at which the force changes sign for $x_1 > 0$ and $x_1 < 0$, respectively (dotted); the critical trajectories $BL+$ and $BR-$, obtained by solving the van der Pol equations backward in time from the leftmost $(-x_{\ell c}^{\max}, 0)$ point with $F(0) = +K$ and rightmost point $(+x_{\ell c}^{\max}, 0)$ with $F(0) = -K$, respectively (dashed). Red and blue trajectory arcs correspond to forces $+K$ and $-K$, respectively.

With the final sign of the force completely determined, along with the final conditions of the momenta given by Eq. (11), we apply the above described numerical algorithm for a large enough value of the force bound—results are shown in Fig. 1. Since there are no intersections between the plotted trajectories and they are the only ones compatible with PMP, they are the optimal trajectories for any initial point in phase space.

The left panel of Fig. 1 shows four different regions in phase space, with one-bang or two-bang optimal controls. The regions are delimited by the following curves: the limit cycle, the critical trajectory $BL+$, the critical trajectory $BR-$, and the switching curves $S\pm$, as described in the caption. It is worth stressing that the switching curves $S\pm$ are not trajectories, but the locus of points at which the force changes sign, i.e. $p_2 = 0$, over the optimal trajectories. Regarding the optimal control's structure, we have: (i) two bangs with time order $(-K, +K)$, above and to the right of the curves $S+$ and $BR-$; (ii) one bang with $F(t) = +K$ between $S+$ and $BL+$, (iii) one bang with $F(t) = -K$ between $S-$ and $BR-$; (iv) two bangs with time order $(+K, -K)$ below and to the left of $BL+$ and $S-$. Note that two bangs are always necessary for initial points on the x_1 -axis.

The structure above is robust for large enough K , such that the critical trajectories $BL+$ and $BR-$ do not intersect the x_1 -axis and thus are one-bang trajectories with no switching points. In the following, we focus the discussion on the behaviour of the $BL+$ trajectory, due to the symmetry of the problem. As K is decreased, there appears a critical value K_{c1} below which $BL+$ intersect the x_1 axis once: this intersection point $x_{c1}(K)$ is a switching

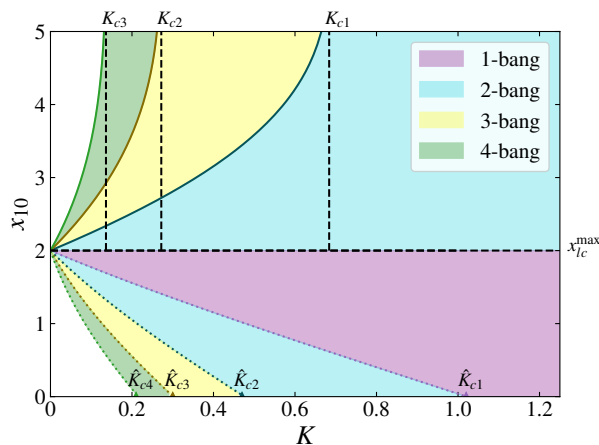


FIG. 2. Phase diagram for the number of bangs in the optimal control in the (K, x_{10}) plane, for initial points on the x_1 -axis. Color code is the same as in Fig. 1. Different regions are delimited by the critical solid (dotted) lines $x_{cn}(K)$ ($\hat{x}_{cn}(K)$) for initial points outside (inside) the limit cycle: to their right, we have $n + 1$ (n) bangs; to their left, we have $n + 2$ ($n + 1$) bangs; over them, we have a critical trajectory, either BL+ or BR-, with n bangs. Critical lines with $n > 4$ are not shown.

point, due to result 3. Prolonging BL+ beyond $x_{c1}(K)$ needs two bangs. If we keep decreasing K , another critical value K_{c2} appears, below which the trajectory BL+ intersect the x_1 -axis twice, at $x_{c1}(K)$ and $-x_{c2}(K)$. Prolonging BL+ beyond $-x_{c2}(K)$ needs three bangs, and so on. Note that we have defined all $x_{cn}(K)$ as positive.

The above is the signature of the emergence of more complex optimal protocols, with a larger number of bangs, as K is decreased. Indeed, the curves $x_{cn}(K)$ are fundamental to understand the complex structure of the optimal control as K is lowered. Figure 2 shows a phase diagram for the number of bangs in the optimal control for initial points on the x_1 -axis, in which the curves $x_{cn}(K)$ delimit the different regions for $x_{10} > x_{lc}^{\max}$.

Summarising, for $K_{c,n+1} < K < K_{cn}$, the critical trajectory BL+ intersects the x_1 axis at n points and the maximum number of bangs for initial points lying on the x_1 -axis is $n + 2$ [56]. Interestingly, $n + 2$ is the maximum number of bangs required to optimally connect any initial phase space point to the limit cycle. The right panel of Fig. 1 illustrates the specific case $K = 0.2$, such that $K_{c3} < K < K_{c2}$, which entails that the maximum number of bangs is four. It is clearly observed that the critical trajectories BL+ and BR- intersect the x_1 -axis at two points: x_{c1} and $-x_{c2}$ for the former, and the symmetric $-x_{c1}$ and x_{c2} for the latter. These points separate different intervals in the x_1 -axis. For the x_1 -axis points closest to the limit cycle, $x_{lc}^{\max} < x_1 < x_{c1}$, two bangs are still enough, as for larger values of K . For $x_1 = x_{c1}$, the optimal control corresponds to the BL+ trajectory and thus have only one bang. For $x_{c1} < x < x_{c2}$, three bangs

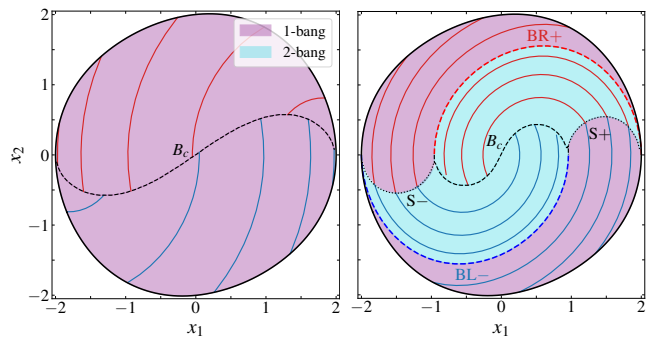


FIG. 3. Optimal trajectories for initial phase space points inside the limit cycle. Force bounds are $K = 2$ (left) and $K = 0.5$ (right). The number of bangs required to connect any initial point to the limit cycle is: (left) always one; (right) one or two, depending on the initial point. In addition to the switching curves S_{\pm} and the critical trajectories BL+ and BR-, analogous to those in Fig. 1, we have plotted the coexistence curve B_c (black dashed), at which the intersecting one-bang trajectories give the same connection time.

are necessary. For $x_1 = x_{c2}$, the optimal control corresponds to the BR- trajectory and thus have two bangs: one bang corresponds to the arc between the final point and $(-x_{1c}, 0)$, and the other to the arc between $(-x_{1c}, 0)$ and $(x_{2c}, 0)$. Finally, for the points furthest from the limit cycle, $x_1 > x_{2c}$, four bangs are needed. Indeed, four is the maximum number of bangs from any phase space point.

Interior points– For points inside the limit cycle, result 4 gives: (i) $\text{sgn}(F_f) = \text{sgn}(x_{2f})$ if $x_{2f} \neq 0$, $\text{sgn}(F_f) = \text{sgn}(x_{1f})$ if $x_{2f} = 0$. While seemingly simpler due to being a finite region, this case is slightly more complex than that for exterior points: trajectories reword from different points on the limit cycle may intersect. As a consequence, there may be more than one trajectory starting from an interior point that fulfils PMP. In that case, to identify the optimal trajectory, we must compare the connection times among all candidate trajectories and select the fastest one. Therefore, a coexistence curve emerges, given by the locus of points at which the fastest synchronisation is degenerate.

For $x_{10} < x_{lc}^{\max}$, Fig. 2 illustrates the critical curves $\hat{x}_{cn}(K)$ governing the optimal control structure inside the limit cycle. Analogously to the case of exterior points, these critical curves are determined by the intersection points with the x_1 -axis of the inside critical trajectory ending at $(-x_{lc}^{\max}, 0)$, as a function of K . In Fig. 3, we observe that (i) one bang is enough for any interior point for $K = 2$ (left panel) (ii) either one or two bangs are necessary for $K = 0.5$ (right panel), consistently with the phase diagram in Fig. 2. Smaller values of K would involve an increasingly larger number of bangs.

We present the minimum connection time as a function of the force in Fig. 4. As the bound in the force K decreases, the connection time consistently increases.

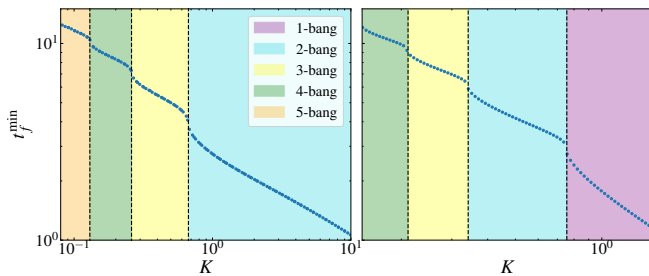


FIG. 4. Minimum connection time as a function of the force bound. Specifically, we have chosen two initial points on the x_1 -axis, one exterior $(5, 0)$ (left) and one interior $(1, 0)$ (right). In both panels, the vertical lines correspond to the values K^* such that $x_{cn}(K^*) = x_{10}$ (left) and $\hat{x}_{cn}(K^*) = x_{10}$ (right). The minimum connection time is continuous at these critical values K^* , but its first derivative with respect to K is not.

The discontinuous derivative of the minimum connection time at the critical values K_{cn} (left, exterior point) and \hat{K}_{cn} (right, interior point) is a consequence of the change in the number of bangs of the optimal protocol thereat, which was illustrated in Fig. 2.

Conclusions– In this Letter, we have solved the minimum-time synchronisation problem to the Liénard equation’s limit cycle. Leveraging Pontryagin’s Maximum Principle, we have derived general analytical results, 1–4, that have been instrumental for developing a robust backward-integration algorithm for finding numerical solutions.

Our application of such general framework to the paradigmatic case of the van der Pol oscillator has revealed detailed insights of the optimal control structure across the whole phase space. As the force bound K decreases or the initial condition moves further from the limit cycle, both the complexity of the optimal control and the minimum synchronisation time increase. This behaviour is intuitively sound, as greater constraints on the system lead to more intricate trajectories and longer connection times.

A crucial point of our analysis is the key role played by “critical trajectories,” i.e. trajectories reword from the extreme points of the limit cycle. They define critical K values, both for points outside and inside the limit cycle, which ultimately determine the maximum number of control bangs required for the optimal connection.

The results presented here pave the way for future research in synchronisation problems. Further extension of our analytical results, e.g. by finding analytical expressions for the critical values of K and the corresponding critical curves $x_{cn}(K)$ and $\hat{x}_{cn}(K)$, is an interesting prospect. Also, given the relevance of synchronisation problems and self-sustained oscillations across numerous fields, applying the ideas introduced here to more complex and realistic models is another promising avenue for exploration.

Acknowledgments– All authors acknowledge financial support from Grant ProyExcel_00796 funded by Junta de Andalucía’s PAIDI 2020 program. CAP and AP acknowledge financial support from the applied research and innovation Project PPIT2024-31833, cofunded by EU–Ministerio de Hacienda y Función Pública–Fondos Europeos–Junta de Andalucía–Consejería de Universidad, Investigación e Innovación. CRM acknowledges support from Ministry of Science, Innovation and Universities FPU programme through Grant FPU22/01151.

Data Availability Statement– The Python codes employed for generating the data are openly available in the GitHub page of University of Sevilla’s FINE research group.

- [1] J.-M. Ginoux and C. Letellier, Van der Pol and the history of relaxation oscillations: Toward the emergence of a concept, *Chaos: An Interdisciplinary Journal of Non-linear Science* **22**, 023120 (2012).
- [2] A. Jenkins, Self-oscillation, *Physics Reports* **525**, 167 (2013).
- [3] A. Gomez-Marin, J. Garcia-Ojalvo, and J. M. Sancho, Self-Sustained Spatiotemporal Oscillations Induced by Membrane-Bulk Coupling, *Physical Review Letters* **98**, 168303 (2007).
- [4] L. G. Arnaut and S. Ibáñez, Self-sustained oscillations and global climate changes, *Scientific Reports* **10**, 11200 (2020).
- [5] D. B. Brückner, A. Fink, C. Schreiber, P. J. F. Röttgermann, J. O. Rädler, and C. P. Broedersz, Stochastic nonlinear dynamics of confined cell migration in two-state systems, *Nature Physics* **15**, 595 (2019).
- [6] J.-C. Leloup, D. Gonze, and A. Goldbeter, Limit Cycle Models for Circadian Rhythms Based on Transcriptional Regulation in *Drosophila* and *Neurospora*, *Journal of Biological Rhythms* **14**, 433 (1999).
- [7] T. Roenneberg, E. J. Chua, R. Bernardo, and E. Mendoza, Modelling Biological Rhythms, *Current Biology* **18**, R826 (2008).
- [8] M. Seki and H. Ito, Evolution of self-sustained circadian rhythms is facilitated by seasonal change of daylight, *Proceedings of the Royal Society B: Biological Sciences* **289**, 20220577 (2022).
- [9] Z. Hu, Y. Li, and J.-a. Lv, Phototunable self-oscillating system driven by a self-winding fiber actuator, *Nature Communications* **12**, 3211 (2021).
- [10] B. Zhang, Y. Yan, X. Dong, M. Dykman, and H. Chan, Frequency stabilization of self-sustained oscillations in a sideband-driven electromechanical resonator, *Physical Review Applied* **22**, 034072 (2024).
- [11] B. Zhang, P. Y. Chan, X. Dong, F. Sun, and H. B. Chan, Slow onset of self-sustained oscillations in a fluctuating sideband-driven electromechanical resonator, *Scientific Reports* **15**, 18965 (2025).
- [12] Y. Kawai, J. Park, and M. Asada, Reservoir computing using self-sustained oscillations in a locally connected neural network, *Scientific Reports* **13**, 15532 (2023).
- [13] Y. Liu, J. Wu, K. Xu, and M. Zheng, Recovery of acti-

- vation propagation and self-sustained oscillation abilities in stroke brain networks, *Physical Review E* **111**, 034309 (2025).
- [14] J. Tabanera-Bravo, F. Vigneau, J. Monsel, K. Aggarwal, L. Bresque, F. Fedele, F. Cerisola, G. A. D. Briggs, J. Anders, A. Auffèves, J. M. R. Parrondo, and N. Ares, Stability of long-sustained oscillations induced by electron tunneling, *Physical Review Research* **6**, 013291 (2024).
- [15] S. H. Strogatz, *Nonlinear Dynamics and Chaos: With Applications to Physics, Biology, Chemistry, and Engineering*, 3rd ed. (Chapman and Hall/CRC, Boca Raton, 2024).
- [16] B. Van Der Pol, LXXXVIII. On “relaxation-oscillations”, *The London, Edinburgh, and Dublin Philosophical Magazine and Journal of Science* **2**, 978 (1926).
- [17] J.-H. He, Determination of Limit Cycles for Strongly Nonlinear Oscillators, *Physical Review Letters* **90**, 174301 (2003).
- [18] D. Guéry-Odelin, A. Ruschhaupt, A. Kiely, E. Torrontegui, S. Martínez-Garaot, and J. G. Muga, Shortcuts to adiabaticity: Concepts, methods, and applications, *Reviews of Modern Physics* **91**, 045001 (2019).
- [19] D. Guéry-Odelin, C. Jarzynski, C. A. Plata, A. Prados, and E. Trizac, Driving rapidly while remaining in control: classical shortcuts from Hamiltonian to stochastic dynamics, *Reports on Progress in Physics* **86**, 035902 (2023).
- [20] F. Impens and D. Guéry-Odelin, Shortcut to synchronization in classical and quantum systems, *Scientific Reports* **13**, 453 (2023).
- [21] C. Ríos-Monje, C. A. Plata, D. Guéry-Odelin, and A. Prados, Optimal synchronization to a limit cycle, *Chaos: An Interdisciplinary Journal of Nonlinear Science* **34**, 103146 (2024).
- [22] A. Gomez-Marin, T. Schmiedl, and U. Seifert, Optimal protocols for minimal work processes in underdamped stochastic thermodynamics, *The Journal of Chemical Physics* **129**, 024114 (2008).
- [23] M. Baldovin, I. B. Yedder, C. A. Plata, D. Raynal, L. Rondin, E. Trizac, and A. Prados, Optimal control of levitated nanoparticles through finite-stiffness confinement (2024), arXiv:2408.00043 [cond-mat].
- [24] S. Deffner and S. Campbell, Quantum speed limits: from Heisenberg’s uncertainty principle to optimal quantum control, *Journal of Physics A: Mathematical and Theoretical* **50**, 453001 (2017).
- [25] U. Boscain, M. Sigalotti, and D. Sugny, Introduction to the Pontryagin Maximum Principle for Quantum Optimal Control, *PRX Quantum* **2**, 030203 (2021).
- [26] E. Dionis and D. Sugny, Time-optimal control of two-level quantum systems by piecewise constant pulses, *Physical Review A* **107**, 032613 (2023).
- [27] H. Fanchiotti, C. A. G. Canal, M. Mayosky, A. Pérez, and A. Veiga, Quantum and classical dynamics correspondence and the brachistochrone problem, *Physical Review A* **110**, 042219 (2024).
- [28] O. Morandi, S. Nicoletti, V. Gavryusev, and L. Fallani, Optimal control in phase space applied to minimal-time transfer of thermal atoms in optical traps, *Physical Review A* **111**, 063312 (2025).
- [29] P. Sun, Y. Liu, and X. Huang, Exploring the brachistochrone (shortest-time) path in fire spread, *Scientific Reports* **12**, 13600 (2022).
- [30] E. Fernandez-Cara and I. Marín-Gayte, Analysis and Numerical Solution of Some Minimal Time Control Problems (2025).
- [31] A. Patrón, A. Prados, and C. A. Plata, Thermal brachistochrone for harmonically confined Brownian particles, *The European Physical Journal Plus* **137**, 1011 (2022).
- [32] A. Patrón, C. A. Plata, and A. Prados, Minimum time connection between non-equilibrium steady states: the Brownian gyrator, *Journal of Physics A: Mathematical and Theoretical* **57**, 495004 (2024).
- [33] L. S. Pontryagin, *Mathematical Theory of Optimal Processes* (CRC Press, 1987).
- [34] D. Liberzon, *Calculus of Variations and Optimal Control Theory: A Concise Introduction* (Princeton University Press, Princeton and Oxford, 2012).
- [35] V. K. Chandrasekar, M. Senthilvelan, and M. Lakshmanan, Unusual Liénard-type nonlinear oscillator, *Physical Review E* **72**, 066203 (2005).
- [36] R. Iacono and F. Russo, Class of solvable nonlinear oscillators with isochronous orbits, *Physical Review E* **83**, 027601 (2011).
- [37] M. Messias and M. R. Alves Gouveia, Time-periodic perturbation of a Liénard equation with an unbounded homoclinic loop, *Physica D: Nonlinear Phenomena* **240**, 1402 (2011).
- [38] S. Ghosh and D. S. Ray, Liénard-type chemical oscillator, *The European Physical Journal B* **87**, 65 (2014).
- [39] T. Shah, R. Chattopadhyay, K. Vaidya, and S. Chakraborty, Conservative perturbation theory for nonconservative systems, *Physical Review E* **92**, 062927 (2015).
- [40] N. Turner, P. V. E. McClintock, and A. Stefanovska, Maximum amplitude of limit cycles in Liénard systems, *Physical Review E* **91**, 012927 (2015).
- [41] J. Giné, Liénard Equation and Its Generalizations, *International Journal of Bifurcation and Chaos* **27**, 1750081 (2017).
- [42] S. L. Kingston, K. Thamilaran, P. Pal, U. Feudel, and S. K. Dana, Extreme events in the forced Liénard system, *Physical Review E* **96**, 052204 (2017).
- [43] R. Suresh and V. K. Chandrasekar, Influence of time-delay feedback on extreme events in a forced Liénard system, *Physical Review E* **98**, 052211 (2018).
- [44] A. Mishra, S. Saha, and S. K. Dana, Chimeras in globally coupled oscillators: A review, *Chaos: An Interdisciplinary Journal of Nonlinear Science* **33**, 092101 (2023).
- [45] Specifically, the conditions are [15]: (i) $V(x)$ is a confining potential with only one minimum at $x = 0$, and (ii) the function $\xi(x) = \int_0^x h(x')dx'$ has the properties: (a) $\xi(x)$ has only one positive zero at $x = a$, with $\xi(x) < 0$ for $0 < x < a$ and $\xi(x) > 0$ for $x > a$, and (b) $\xi(x)$ is non-decreasing for $x > a$, with $\lim_{x \rightarrow \infty} \xi(x) = +\infty$.
- [46] R. FitzHugh, Impulses and Physiological States in Theoretical Models of Nerve Membrane, *Biophysical Journal* **1**, 445 (1961).
- [47] J. Nagumo, S. Arimoto, and S. Yoshizawa, An Active Pulse Transmission Line Simulating Nerve Axon, *Proceedings of the IRE* **50**, 2061 (1962).
- [48] J. H. E. Cartwright, V. M. Eguíluz, E. Hernández-García, and O. Piro, Dynamics of Elastic Excitable Media, *International Journal of Bifurcation and Chaos* **09**, 2197 (1999).
- [49] P. D. Mininni, D. O. Gómez, and G. B. Mindlin, Stochastic Relaxation Oscillator Model for the Solar Cycle, *Physical Review Letters* **85**, 5476 (2000).

- [50] P. Romanczuk, M. Bär, W. Ebeling, B. Lindner, and L. Schimansky-Geier, Active Brownian particles: From individual to collective stochastic dynamics, *The European Physical Journal Special Topics* **202**, 1 (2012).
- [51] C. Zhang, M. Kim, J. Wang, and C.-M. Hu, Van der Pol–Duffing oscillator and its application to gain-driven light-matter interaction, *Physical Review Applied* **22**, 014034 (2024).
- [52] T. E. Lee and H. R. Sadeghpour, Quantum Synchronization of Quantum van der Pol Oscillators with Trapped Ions, *Physical Review Letters* **111**, 234101 (2013).
- [53] L. Ben Arosh, M. C. Cross, and R. Lifshitz, Quantum limit cycles and the Rayleigh and van der Pol oscillators, *Physical Review Research* **3**, 013130 (2021).
- [54] N. Thomas and M. Senthilvelan, Quantum synchronization in quadratically coupled quantum van der Pol oscillators, *Physical Review A* **106**, 012422 (2022).
- [55] C. W. Wächtler and G. Platero, Topological synchronization of quantum van der Pol oscillators, *Physical Review Research* **5**, 023021 (2023).
- [56] We are defining $K_{c0} = \infty$ to employ this equation for $n = 0$, which is consistent with defining $x_{c0}(K) = x_{\ell c}^{\max}$.
- [57] G. Leitmann, *Topics in optimization*, Mathematics in Science and Engineering No. 31 (Academic Press, Inc., New York, 1967).
- [58] M. I. Zelikin and V. F. Borisov, Singular Optimal Regimes in Problems of Mathematical Economics, *Journal of Mathematical Sciences* **130**, 4409 (2005).

End Matter

Appendix: Derivation of results 1–4 from PMP—In this section, we detail the proofs of the analytical results 1–4.

Result 1: the optimal control is bang-bang—To prove this, we use property (ii) of PMP, which states that the Hamiltonian is maximum with respect the control at the optimal one. Since the control set is bounded, $F(t) \in [-K, K]$, the maximum of \mathcal{H} may lie either (i) in the open interval $(-K, K)$ or (ii) at the boundaries of the control set, i.e. $F(t) = \pm K$. In the first case, bringing to bear Eq. (6), we get

$$\frac{\partial \mathcal{H}}{\partial F} = 0 \Rightarrow p_2 = 0. \quad (12)$$

Due to the linear dependence of the Hamiltonian on F , this is a singular optimal control problem and Eq. (12) does not give us any information about the optimal control. Therefore, we apply the Kelley condition [57, 58] to get further information about the control. We start by differentiating Eq. (12) with respect to time:

$$\frac{d}{dt} \left(\frac{\partial \mathcal{H}}{\partial F} \right) = 0 \Rightarrow \dot{p}_2 = 0. \quad (13)$$

Taking into account p_2 equation in Eq. (7), we get

$$0 = -p_1 + \mu h(x_1) p_2 \stackrel{0}{=} -p_1. \quad (14)$$

Therefore, if there is a time interval (t_1, t_2) where Eq. (12) is satisfied, we conclude that $\mathbf{p} = \mathbf{0}$ therein. That would

mean, using Eq. (8), that also $p_0 = 0$ and $\{\mathbf{p}, p_0\} = \{\mathbf{0}, 0\}$ for all $t \in (t_1, t_2)$. But this is incompatible with PMP and case (i) has to be discarded. Therefore, the only scenario is (ii); over the possible optimal control we have $F(t) = \pm K$. The sign of the control is determined by the sign of the coefficient of F in \mathcal{H} , which is p_2 , which leads to Eq. (10).

Result 2: final value of the costate—Let us know focus on the transversality condition, Eq. (9), and Eq. (8) at the final time t_f ,

$$p_{1f} x_{2f} + p_{2f} [-\mu h(x_{1f}) x_{2f} - V'(x_{1f})] = 0, \quad (15a)$$

$$p_{1f} x_{2f} + p_{2f} [-\mu h(x_{1f}) x_{2f} - V'(x_{1f}) + F_f] + p_0 = 0, \quad (15b)$$

respectively, where $\mathbf{p}^T(t_f) = (p_{1f}, p_{2f})$ and $F_f \equiv F(t_f)$. Combining these two equations yields

$$p_{2f} F_f + p_0 = 0. \quad (16)$$

The limit cycle of the Liénard equation has two extreme points $(\pm x_{\ell c}^{\max}, 0)$, at which x_1 is either maximum or minimum and thus $\dot{x}_1 = x_2$ vanishes. It is only at these points of the limit cycle that the vector \mathbf{d} of its tangent space is vertical and x_2 vanishes. On the one hand, if the final point (x_{1f}, x_{2f}) is not one of the extreme points, then we have that $p_{2f} \neq 0$ —because the final vector of momenta is not horizontal—and Eq. (16) entails that $p_0 \neq 0$. Normalising it to $p_0 = -1$, as usual in optimal control theory [33, 34], we obtain Eq. (11a) in result 2. On the other hand, if the final point (x_{1f}, x_{2f}) is one of the extreme points $(\pm x_{\ell c}^{\max}, 0)$, then we have that $p_{2f} = 0$ and Eq. (16) now implies $p_0 = 0$: we need $p_{1f} \neq 0$ to fulfil PMP. The sign of p_{1f} is determined by the sign of F_f . Considering Eq. (7) for p_2 , with $p_{2f} = 0$, we get

$$\dot{p}_{2f} = -p_{1f} \quad (17)$$

Now if we assume $F_f > 0$, then, by Eq. (10), $p_{2f}^- > 0$. Since $p_{2f} = 0$, this implies $\dot{p}_{2f} < 0$ that in turn entails $p_{1f} > 0$. Conversely, if $F_f < 0$, we get the opposite result. This gives Eq. (11b) in result 2.

Result 4: sign of the final bang—Bringing to bear the final value of the force $F(t_f) = F_f$, we can rewind the evolution equations from the final point over the limit cycle $\mathbf{x}_f^T = (x_{1f}, x_{2f})$. We have taken $\chi_{\ell c} > 0$ (< 0) for phase plane points lying outside (inside) the limit cycle. Therefore, $\nabla \chi_{\ell c}(x_{1f}, x_{2f})$ points outwards from limit cycle, and since the gradient is perpendicular to the tangent to the limit cycle, we write

$$\nabla \chi_{\ell c}(\mathbf{x}_f)^T = c_f (\mu h(x_{1f}) x_{2f} + V'(x_{1f}), x_{2f}), \quad c_f > 0. \quad (18)$$

Note that c_f may depend on \mathbf{x}_f , $c_f = c(\mathbf{x}_f)$.

Now we consider an infinitesimal time interval $(t_f - \varepsilon, t_f)$ and the corresponding phase space point $\mathbf{x}_f^- = (x_{1f}^-, x_{2f}^-)$ at $t_f - \varepsilon$. Up to first order in ε , we have

$$x_{1f}^- = x_{1f} - \varepsilon x_{2f}, \quad (19a)$$

$$x_{2f}^- = x_{2f} - \varepsilon [-\mu h(x_{1f})x_{2f} - V'(x_{1f}) + F_f], \quad (19b)$$

in which we have neglected $O(\varepsilon^2)$ terms. Using Eqs. (19) to expand $\chi_{\ell c}$ at \mathbf{x}_f yields

$$\chi_{\ell c}(\mathbf{x}_f^-) = -\varepsilon F_f \left. \frac{\partial \chi_{\ell c}}{\partial x_2} \right|_{\mathbf{x}_f} = -\varepsilon c_f x_{2f} F_f, \quad (20)$$

where we have omitted $O(\varepsilon^2)$ terms. For $x_{2f} \neq 0$, Eq. (20) entails that $x_{2f} F_f < 0$ when reaching the limit cycle from the outside (exterior initial point), whereas $x_{2f} F_f > 0$ when reaching the limit cycle from the inside (interior initial point)—in agreement with result 4.

We have to study separately the case $x_{2f} = 0$, in which the first order approximation in Eq. (20) vanishes. This corresponds to the critical trajectories in which $x_{1f} = \pm x_{\ell c}^{\max}$. Expanding $\chi_{\ell c}$ from these extreme points of the

limit cycle to second order in ε gives

$$\chi_{\ell c}(\mathbf{x}_f^-) = -\frac{\varepsilon}{2} c_f x_{2f}^- F_f, \quad (21)$$

once more using Eq. (19). For initial points outside the limit cycle, for which $\chi_{\ell c} > 0$, we get: (i) if $x_{2f}^- < 0$, then $F_f > 0$ and the last bang must be $F(t) = +K$; (ii) if $x_{2f} = 0$ but $x_{2f}^- > 0$, then $F_f < 0$ and the last bang must be $F(t) = -K$. For initial points inside the limit cycle, the sign of the bangs is reversed, taking into account that $\chi_{\ell c} < 0$. This completes the proof of our result 4.

Equation (19b) leads to

$$x_{2f} = 0 \implies x_{2f}^- = \varepsilon [V'(\pm x_{\ell c}^{\max}) - F_f]. \quad (22)$$

Therefore, for small values of the bound, such that $V'(x_{\ell c}^{\max}) > K$, the sign of x_{2f}^- is perfectly determined: negative at $(-x_{\ell c}^{\max}, 0)$ and positive at $(x_{\ell c}^{\max}, 0)$. This leads to the critical trajectories BL+ and BR− in the main text. For larger values of the bound, $V'(x_{\ell c}^{\max}) < K$, x_{2f}^- may have both signs and there may exist critical trajectories BL− (with $x_{2f}^- > 0$) and BR+ (with $x_{2f}^- < 0$), in addition to the trajectories BL+ and BR−. However, the trajectories BL− and BR+ consist of points that belong to other candidates to optimal trajectories with shorter synchronisation times, and therefore they can be discarded.